ELSEVIER

Marine Geology 119 (1994) 57–65

MARINE GEOLOGY
INTERNATIONAL JOURNAL OF MARINE GEOLOGY, GEOCHEMISTRY AND GEOPHYSICS

Rotary sidescan images of nearshore bedform evolution during a storm

Alex E. Hay, Douglas J. Wilson

Department of Physics, Memorial University of Newfoundland St. John's, Nfld. A1B 3X7, Canada

(Received June 7, 1993; revision accepted February 22, 1994)

Abstract

High resolution acoustic images are presented of bedform development on the crest of a nearshore bar during a storm. The images were obtained using a 2.25 MHz rotating sidescan sonar. The sonar system provides a continuous record of the evolution of the bedform field through time, within a 10-m diameter field of view. The images document the occurrence of ripples, cross ripples, and megaripples. During the waning stages of the storm, transitions among ripple types occurred on time scales of 1–3 h, beginning with flat bed and culminating in highly 3-D short-crested ripples.

1. Introduction

The development and movement of bedforms is an important component of both the nearshore sand transport problem, and the problem of interpreting the sedimentary record in terms of coastal sediment transport processes. However, few bedform measurements have been made on submerged bars during conditions of active transport (Allen, 1982b, p. 450). Direct observations by divers are difficult to make during storm events (Miller and Komar, 1980). Observation of the bottom using underwater stereo cameras or video cameras has met with limited success because suspended matter frequently obscures the view of the bottom (see, e.g., Horikawa, 1988).

Acoustic methods of bedform measurement should in principle be less sensitive to the presence of suspended sediment, and have shown promise. Dingler and Inman (1976) used a track-mounted vertical sounder to obtain 1-D profiles of bed elevation along the 2-m length of the track. Dingler and Clifton (1984) and Greenwood et al. (1993) describe more recent measurements made with this type of system. Bedforms have also been monitored with a horizontally-distributed 2-D array of vertical sounders (Hay and Bowen, 1993). Both types of measurement, linear track and altimeter array, are limited by the 3-D nature of many bedforms, and the spatially inhomogeneous distribution of larger bedform types, megaripples in particular (Clifton, 1976; Allen, 1982a,b). Thus it was felt that a system capable of spatial coverage in more than one dimension extending over distances beyond 1–3 m, and with O (1 cm) spatial resolution, would contribute valuable information which has been difficult to obtain by other means. The system chosen was a rotating fan-beam sonar, with a range of about 5 m. Results from the first field deployment of this system are described below.

2. Experimental setup

The measurements reported here were made on the southeastern shore of Lake Huron at Burley Beach, Ontario in October, 1992. The sidescan sonar used in the experiment is a customized

SSDI 0025-3227(94)00025-G

version of Simrad Mesotech's Model 971. It consists of an underwater transceiver with a fan-beam transducer, driven about a vertical axis by a stepper motor and connected to control and data acquisition electronics onshore via a multielement coaxial cable. The operating characteristics of the sonar are given in Table 1. The sidescan has been incorporated into an upgraded version of RASTRAN System 1 (Hay et al., 1988; Hay and Sheng, 1992). The rotary head was mounted on the shoreward end of the RASTRAN frame at a 50 cm nominal height above bottom, with the transducer beam tilted at 30° below the horizontal (Fig. 1). The frame was located near the crest of a shore-parallel bar in about 1.5 m water depth, approximately 110 m from the shoreline. The bottom sediments at the measurement location consisted of moderately well sorted sand of 200 μm median diameter.

Table 1
Sonar characteristics

Frequency	2.25 MHz
Vertical beamwidth	30°
Horizontal beamwidth	0.8°
Angular step interval	0.45°
Pulse length	10 μs
Range resolution	≈1 cm

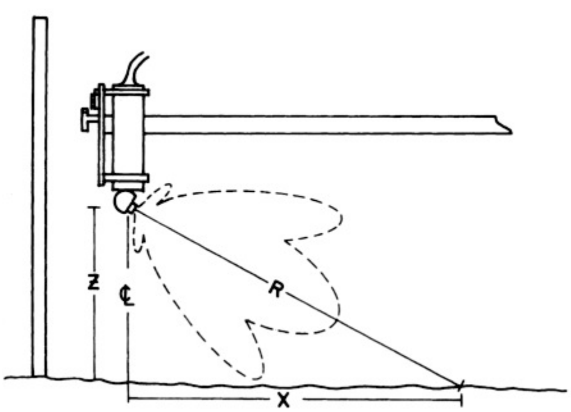

Fig. 1. Side view schematic of a portion of the RASTRAN frame, showing the sidescan sonar head and housing, the beam pattern of the head (at 60 cm range). The sonar head is attached to a horizontal frame, which is supported by vertical posts at the corners. One vertical post is shown on the left. The cantilever support between the frame and the post is not shown (see Fig. 2).

Other sensors were mounted on the frame, including an array of vertical acoustic sounders and Marsh-McBirney electromagnetic current meters. The frame legs and some of the sensors partially obstructed the beam of the rotary sonar, casting shadows in the images. These shadows have been sketched in Fig. 2 and are identified later.

The received signals were first envelope-detected and then acquired digitally at a sampling rate of 200 kHz using RASTRAN's data acquisition system. The time for a full 360° scan was 47 s. Each stored image contains 1.1 MBytes of data. Up to ten consecutive digital images were acquired during a 10-min time window at hourly intervals. The backscatter data were also displayed on a video monitor, and recorded continuously on videotape. Three images, representing a small fraction of the total data set, have been selected for presentation here.

3. Results

Data were collected over the 42-h duration of the storm, which started abruptly at about 0600 h

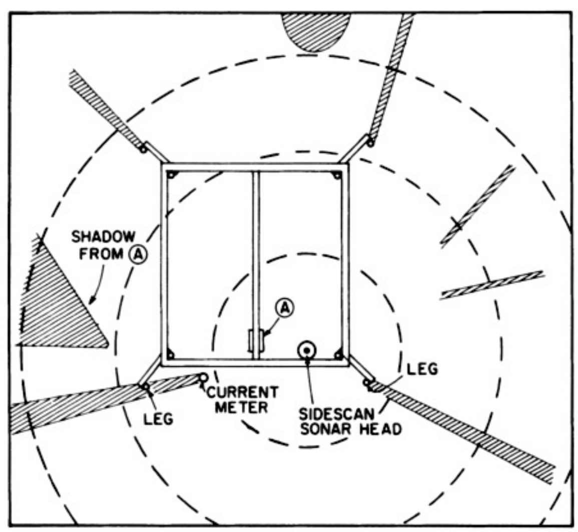

Fig. 2. Plan view of the RASTRAN frame. The frame is 2 × 2 m, and constructed from 6.5-cm aluminum angle. The 5-cm diameter corner posts (legs) are 2.2 m apart. Dashed rings denote distance from the rotating sonar head in 1-m range increments. Shadows cast by various parts of the frame and sensors (see text) are indicated.

on October 24, peaked at about 1400 h, and gradually abated over the next 34 h. During the initial period of the storm, pronounced changes in local mean bed elevation occurred as a result of bar development and migration. In this paper, results are presented from the period following peak storm intensity, when the local bed elevation was comparatively stable, on October 25. The period of the incident surface gravity waves during this time was 4 to 5 s. Fluid velocities from the flowmeter 70 cm above the bed (Fig. 2) are given in Table 2. Mean cross-shore currents were small, 1–2 cm/s, and were directed offshore. The longshore current $\bar{V}$ was directed westward (to the left in the images), and decreased in magnitude from 48 to 10 cm/s. Significant wave orbital velocities $u_s[=2\sqrt{u_{rms}^2+v_{rms}^2}$, where u_{rms} and v_{rms} are the root-mean-square velocities: that is, the square root of the variance of the velocity records (see Guza and Thornton, 1980)] dropped from 98 to 47 cm/s. The decay in the forcing is therefore evident in both the longshore current and in the wave velocities.

A measure of the bottom skin friction is given by the grain roughness Shields parameter $\theta_{2.5}$:

$$\theta_{2.5}=f_{2.5}u_s/2(s-1)gd_{50} \tag{1}$$

where d_{50} is the median grain diameter, $f_{2.5}$ is the wave friction factor based on 2.5 d_{50}, s is the grain specific gravity, and g is the acceleration due to gravity (see Nielsen, 1981, 1992, p. 105). The seabed images to be presented were acquired at the (last three) times listed in Table 2, for which the values of $\theta_{2.5}$ ranged from 0.89 to 0.34. These values fall in the upper end of the intermediate strength flow regime $0.05 \leqslant \theta_{2.5} \leqslant 1.0$ defined by Nielsen (1992, p. 105), in which vortex ripples are expected.

The first of the selected rotary sidescan images, acquired at 1638 h, is shown in Fig. 3a. The image is displayed in grey scale, darker areas representing higher acoustic backscatter intensity. The shadows from the frame supports and some of the sensors are readily identified as light areas which appear in the same location in each image, as sketched in Fig. 2. Each of the four 5-cm diameter support legs casts a shadow extending radially outward from the rotary sonar. The large shadow (A) on the left side of the images is cast by another sonar housing. The shadow at the top (offshore side) is from a loop of cable attached to the frame. The two shadows on the middle right are from guy wires running from the frame corners to an anchor post imbedded in the bottom. The shadows provide useful reference points for image interpretation. The images have been slant-range corrected assuming a horizontal bed. The displayed image represents an area of the bottom 10 m across diagonally. The circles represent radial distances along the bottom at 2-m intervals, centred at the point on the bottom directly beneath the sonar head. The high intensity backscatter within 1-m of the centre, and the weaker signal in the 1 to 1.5 m distance interval, are due to the lobes of the transducer beam pattern (Fig. 1).

The image in Fig. 3a shows long-crested shore-

Table 2
Mean and rms velocities at 2-h intervals for the 8-h period preceding the first image, acquired at 1638 h, at the times of each of the three images discussed in the text. u is positive onshore (southward); v is positive longshore (eastward). Also listed are values for the significant wave orbital velocity, u_s; significant wave orbital diameter, $2A=u_sT/\pi$; grain roughness Shield's parameter $\theta_{2.5}$. Values for λ/A, computed from Nielsen's (1981) empirical formula, are shown for the times of the images in Figs. 3–5, and discussed in the text

Time EDT	u_{rms} (cm/s)	$\bar{U}$ (cm/s)	v_{rms} (cm/s)	$\bar{V}$ (cm/s)	u_s (cm/s)	$2A$ (cm)	$\theta_{2.5}$	λ/A
0814	44.1	−1.9	21.3	−48.0	98		1.28–1.35	
1015	44.4	−0.7	18.5	−34.8	96		1.23–1.30	
1217	39.2	0.3	15.5	−25.0	84		0.98–1.03	
1415	35.9	−1.0	13.3	−19.1	77		0.82–0.87	
1638	35.6	−1.3	14.2	−17.5	77	98–123	0.84–0.89	0.081
1841	30.3	−1.5	12.4	−11.3	65	83–103	0.62–0.65	0.096
2138	21.8	−2.4	8.0	−10.0	46	59–73	0.34–0.37	0.148

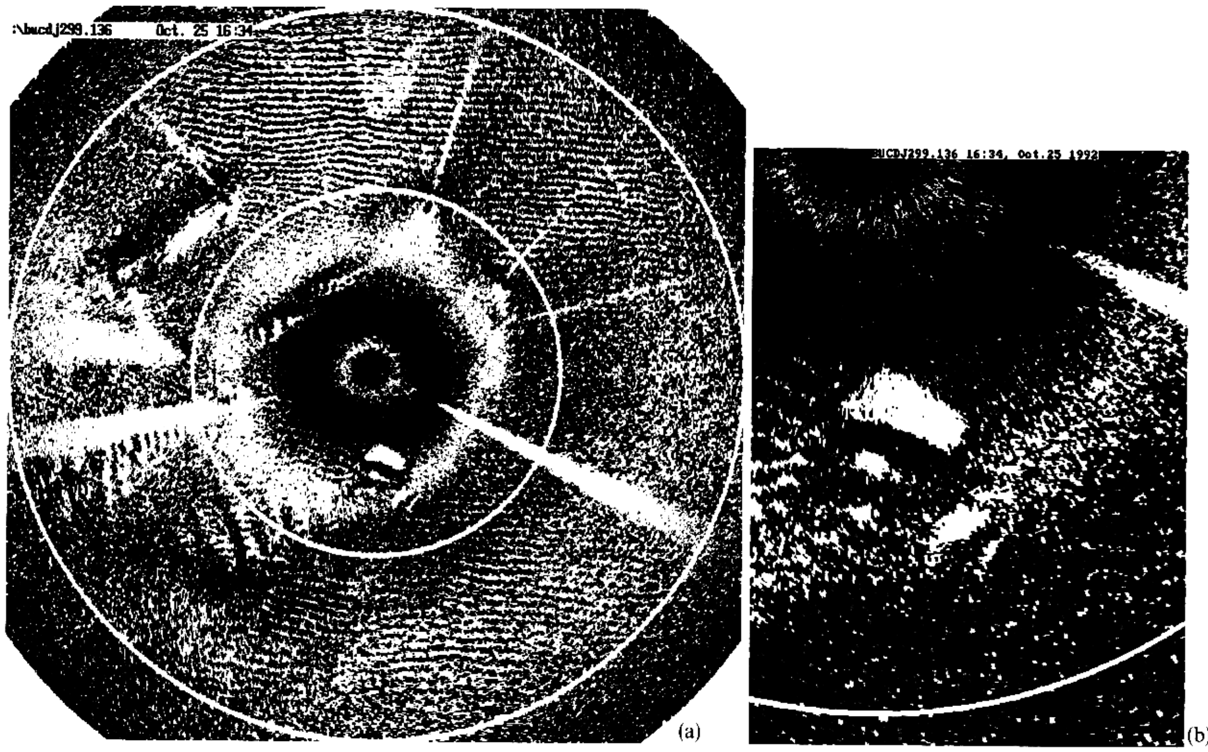

Fig. 3. (a) The first image, at 1634 h on 25 October 1992, showing long-crested, shore-parallel ripples. Note that although ripples do not appear to be present on the left and right sides in the middle of the image, this is because the ripples are aligned parallel to the acoustic beam in these areas, and thus produce no shadows. In this and all subsequent images, the onshore direction is down (south, and positive u), and the positive longshore direction is to the right (east, and positive v). (Run 299.136). (b) Detail from the image in Fig. 3a, showing the megaripple. The letter B at the beginning of the file name is located at the position of the rotary sonar head (i.e. at the centre of the complete image, Fig. 3a.).

parallel ripples, with occasional bifurcations. The average wavelength (λ) of these ripples is 9–10 cm. The significant wave orbital diameter ($2A$) was 100–120 cm for this run (Table 2). The ripple wavelength therefore falls within the range of values given by Miller and Komar (1980) for these orbital diameters (actually near the short wavelength end of this range, near Clifton's (1976) anorbital ripple grouping). Several larger scale bedforms are present. One of these is a crescent-shaped depression (area of low signal intensity) located roughly 1-m shoreward of the sonar head. An expanded view of this crescent-shaped feature is presented in Fig. 3b. The horns of the crescent point toward shore. The horn-to-horn span is about 50 cm. During the ensuing 2 h, this feature migrated a distance of about 1 m shoreward and slightly to the south (leftward in the image), gradually disappearing on the way. The feature has the characteristic dimensions and shape of a lunate megaripple (Clifton et al., 1971).

The second type of larger scale feature is in the lower left quadrant of the first image, to the left of the megaripple. These features have wavelengths of 30–40 cm, with crests aligned roughly 20° off shorenormal, and two hours later had grown to fill the entire field of view (Fig. 4a). Shorter wavelength ripples are still present among the larger scale features, but are inclined with respect to the crests of the longer wavelength bedforms and, except in isolated patches, are no longer shore-parallel. These are cross ripples (Clifton, 1976), with crests of both the longer and shorter ripple sets oriented obliquely to the direction of the incident waves. A more detailed view of the cross-ripples is presented in Fig. 4b. This figure shows a

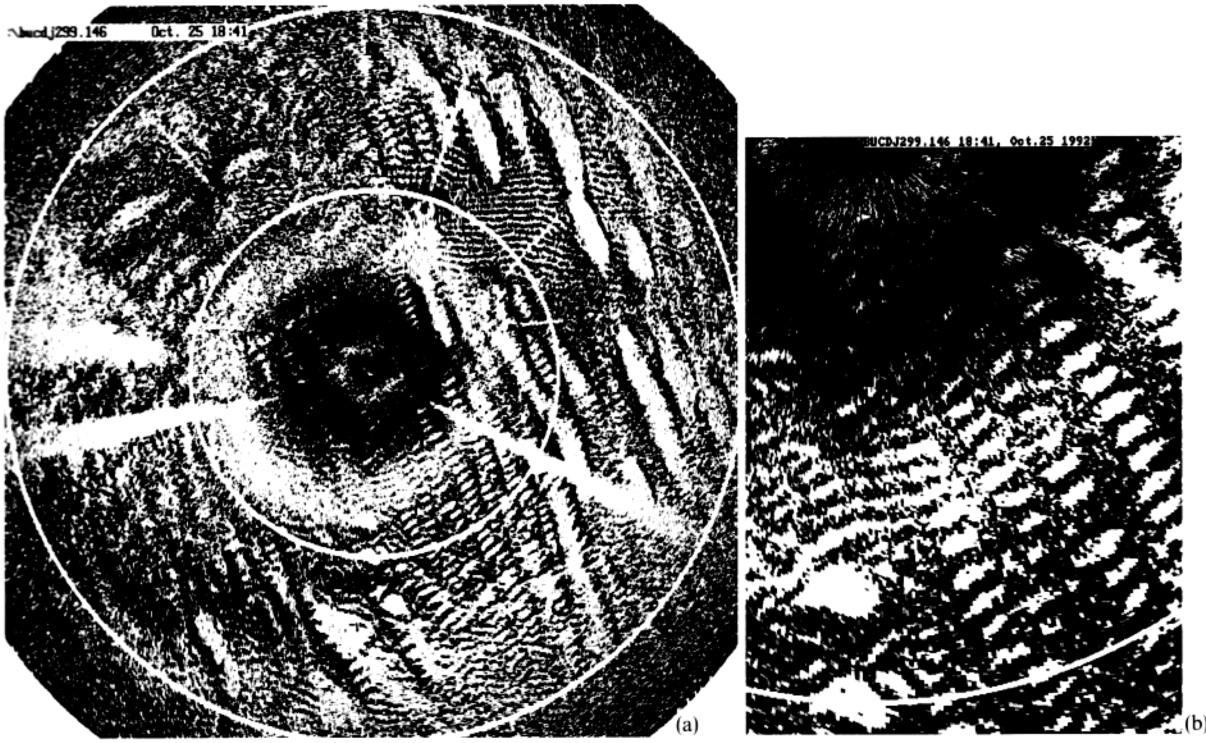

Fig. 4. (a) The second image, at 1841 h on 25 October 1992, showing cross ripples (Run 299.146). (b) Expanded view of the cross ripples in Fig. 4a. Also shown is the megaripple, which has migrated to the southwest of its previous position (Fig. 3b). A companion megaripple appears to have developed nearby (see text). The letter *B* at the beginning of the file name is located at the position of the rotary sonar head (i.e. at the centre of the complete image, Fig. 4a.).

frequent half-wavelength offset of the short ripple component on either side of a long ripple crest.

As shown by the expanded view in Fig. 4b, the megaripple is still present, but is reduced in size (compare Figs. 4b and 3b), and is located roughly 70 cm shoreward of its earlier position. Another lunate feature, possibly a second megaripple, is present directly shoreward on the 2-m circle. Larger lunate features, also resembling megaripples, are located in the upper left quadrant of the image in Fig. 4a, about 3-m from the centre.

The image in Fig. 4a also shows a 20-cm diameter scour pit about the post in the upper right corner of the frame. Scour pits of this size occurred frequently at the support posts during the course of the experiment.

The cross ripples co-existed with patches of 2-D ripples for a period of about two hours. After 3 hours, however, they were replaced by a third bedform type: short-crested, highly 3-D ripples uniformly covering the bed (Fig. 5). Remnants of the long wavelength component of the cross ripples can be seen in the upper right quadrant. These irregular ripple marks remained for the duration of our observations on the night of October 25, a period of about 11 h. They are similar in appearance to the interference ripple marks discussed by Allen (1982a, pp. 435 and 452), which are ascribed to the combined effects either of two intersecting surface wave trains, or of waves and a mean current. Certainly, a mean longshore current was present (Table 2).

4. Discussion

Clifton (1976) presents a conceptual model for the transition among bedform types as a function

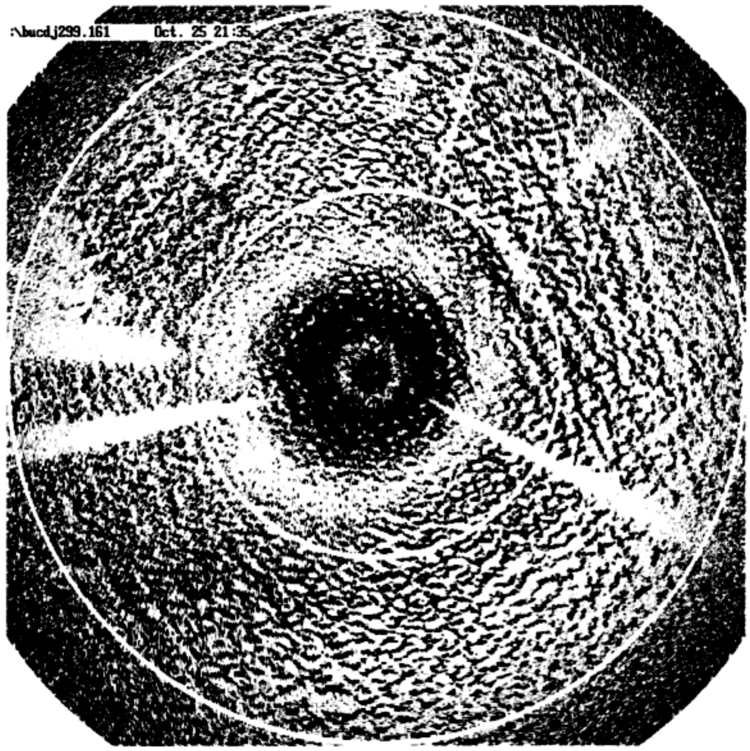

Fig. 5. The third image, at 2135 h on 25 October 1992, showing irregular 3-D ripples (Run 299.161).

of distance offshore. The progression from deep water shoreward is: first, long-crested shore parallel ripples with occasional bifurcations, then irregular short-crested ripples, then cross ripples, then lunate megaripples with crescent horns shoreward, and finally flat bed. This succession of bedform types is associated by Clifton with the progressive increase both in the asymmetry of the oscillatory motion and in the bottom shear stress as the waves shoal toward the beach. Clifton presents his model for a non-barred beach, but it is transferrable to a barred beach, with the bar crest taking the place of the shoreline (Hunter et al., 1979; Nielsen, 1992, p. 130).

We also observe a transition among many of the bedform types discussed by Clifton, but as a function of time at a single offshore location, rather than as a function of distance at a given time. This progression was observed during decay in the wave velocities, and therefore in the bed shear stress, indicating a possible parallel with Clifton's model. The order of progression in the present observations is:

(1) "Flat" bed (no vortex ripples).

(2) Long-crested shore-parallel ripples, with occasional megaripples.

(3) Oblique cross ripples, combined with patchy shore-parallel ripples and occasional megaripples.

(4) Irregular (3-D, short-crested) ripples.

The evidence for Step 1, the flat bed state, is as follows. Conditions were much more energetic during the period preceding the first image shown here. This is demonstrated in Table 2, which shows on the basis of the flowmeter measurements that $\theta_{2.5}$ was well above unity 6–8 h prior to the image in Fig. 3. Flat bed (meaning here the absence of vortex ripples) would therefore be expected (e.g. Nielsen, 1992, p. 131). Furthermore, the longshore current approached 50 cm/s (Table 2), greatly increasing the bed shear stress compared to the effects of waves alone at these times (e.g. Grant and Madsen, 1986). The bed shear stress should therefore have been more than sufficient to prevent the formation of vortex ripples. Also, the sidescan images of the bed during this period are essentially featureless, possibly indicating flat bed, except for the occassional appearance of ripple-like features, which then dissappear in subsequent images, 1 min apart. The disappearance of ripples on short time scales has been reported before. Dingler and Inman (1976) observed that ripples could be wiped out during the passage of wave groups. However, we must point out with respect to our own measurements that, at 2.25 MHz, backscatter from suspended sediment affects the images intermittently, particularly in high energy conditions. (A lower frequency sonar, less sensitive to sand in suspension, may prove useful for bedform monitoring in very energetic conditions.)

Step 2 is the shore-parallel rippled state (Fig. 3). The ratio of ripple wavelength to median grain diameter, λ/D, is about 500 for these ripples. The ratio of wave orbital diameter to grain size, $2A/D$, is about 5000. These ripples therefore lie in the transition region between suborbital and anorbital ripples in Clifton's classification scheme (Clifton, 1976; Clifton and Dingler, 1984, fig. 5). Note that Fig. 3 indicates that ripples and megaripples co-exist. This is consistent with other work. Clifton et al. (1971) found that ripples were superimposed on megaripples, and recent laboratory experiments by Southard et al. (1990) have shown that small 6–8 cm wavelength ripples are superimposed on megaripples formed in 110 μm median diameter sand under high velocity (30–80 cm/s amplitude) oscillatory flows. The small superimposed ripples become increasingly 2-D with increasing velocity amplitude. Southard et al. distinguish between these ripples and vortex ripples, calling them reversing current ripples instead. The ripple wavelength to wave orbital excursion amplitude ratio λ/A is 0.15–0.18 for the ripples in Fig. 3. Nielsen (1981) gives an empirical formula for λ/A in irregular waves:

$$\lambda/A = \exp\left[\frac{693 - 0.37 \ln^8 \psi}{1000 + 0.75 \ln^7 \psi}\right] \quad (2)$$

where ψ is the mobility parameter, given by $2\theta_{2.5}/f_{2.5}$. The observed values are a factor of 2 or so greater than the value predicted by Nielsen's formula (see Table 2).

A similar sequence of events occurred during the 2-h period of time immediately following the abrupt onset of the storm, but in reverse sequence. In this case, the initial state of the bed corresponded to long-crested, bifurcating ripples with wavelengths of 8 cm. These appear to have been orbital ripples, produced by low amplitude waves prior to the onset of the storm. These ripples were rapidly transformed into irregular ripple marks similar to Fig. 5, followed in turn by cross-ripples similar to those in Fig. 4. The bed then appeared to go planar.

A difference between the Clifton progression and our observations is that 2-D long-crested ripples, corresponding to Clifton's farthest offshore (and low bottom stress) bedform, did not reform during the final period of decay of the storm. Our observations indicate that whatever the mechanism responsible for the formation of the irregular ripple pattern, this was the final state of the seabed after the storm. The explanation for this observation may be related to the longshore current, which persisted as the waves decayed (Table 2). The longshore current is not included in Clifton's model, which assumes shorenormal wave incidence. It may also be an effect peculiar to lakes, or to this particular storm event. Presumably, long-crested ripples will form if swell of sufficient amplitude and duration follows the storm. This need not occur in bodies of restricted fetch, like the Great Lakes. Perhaps the wave/current forcing dropped below the threshold of grain movement too rapidly for long-crested ripples to have time to form. This line of thinking raises the more general question of the time lag between a change in the forcing and the resulting adjustment of the bedform field, and how this may depend upon the previous state of the bed.

The Clifton progression is based on SCUBA observations in relatively calm conditions: under long-period swell on the Oregon coast, the "protected" shoreline of Willapa Bay, Washington, and the "relatively calm" southeastern coast of Spain. In contrast, the present measurements were made during a storm, in conditions in which SCUBA observations would have been impossible. Perhaps it is not surprising that in such conditions the bedform field should exhibit more complex behaviour.

Finally, we consider possible effects of the instrument frame on the bedform fields in these images. One such effect, the scour pits around the frame posts, has been mentioned. These pits are roughly 4 post diameters across, similar to the 3 post-diameter pit shown by Allen (1982a, p. 204). The images in Figs. 4 and 5 do not show any other pronounced effects of the frame: the irregular ripples in Fig. 5 are uniformly distributed throughout the field of view; the cross ripples in Fig. 4 are similar in appearance everywhere except on the downstream (left) side, where they are not as clear. This is partly the result of the shadows on this side, and of the megaripples in the upper left corner. There are features in Fig. 3a, however, which look suspiciously like wake effects associated with the longshore current: narrow ripple trains appear on the downstream (left) side of some of the posts, particularly the upper right and lower left. It is known that ripples are generated by bed topography perturbations which can be induced in a variety of ways, including obstacles in the sand (Allen, 1982a, p. 442), and the narrow ripple trains downstream of the posts (in the longshore current sense) may well be artifacts of this kind.

5. Conclusions

The primary intent of this short communication is to demonstrate the usefulness of high resolution rotary sidescan sonars for making measurements of bedforms in nearshore environments during storm events. The technique has a number of advantages. In particular, it is much less sensitive than are optical seabed imaging methods to suspended matter in the water. (It is worth noting perhaps that visual or optical measurements of the seabed were completely impractical at Burley Beach, because of the presence of fine material in suspension, delivered by nearby rivers. Visibility was limited to 10 cm or less.) Furthermore, the seabed can be monitored over an area exceeding 10 m^2. Areal coverage of this order seems to be necessary to allow adequate knowledge of the distribution of different bedform types, particularly the larger scale forms (i.e. megaripples). The fact that the areal coverage extends well beyond the instrument frame is also useful, as the effects of the instrument support structure on the seabed response can then be assessed. Such knowledge is likely to prove important for suspended sediment measurements (Hay and Bowen, 1994). Finally, the technique provides images of the bedform pattern in plan view, and therefore direct information on bedform orientation, on the three-dimensionality of the bedform field, and on bedform migration.

The limitations of the approach remain to be explored. The 5-m maximum range of the present measurements could be improved. Sources of noise in the images, such as scattering from sediments in suspension or from bubbles due to breaking waves, need to be investigated. It should be possible to minimize these effects by the appropriate choice of frequency, and improved signal processing techniques. Information on bedform amplitudes, while not as readily accessible as bedform pattern, is contained in the images (as shadow length, for example), and could be exploited.

The results presented here indicate that the local evolution of the bed involves transformations among 2- and 3-D bedform fields. The transformations occur on time scales of a few hours or less. The different bedform fields can be complex, involving mixtures of bedform types with different characteristic length scales. This has implications for sediment transport modelling. It would appear to be incorrect, for example, to assume a single bedform type during the course of a storm. It also appears that it can be incorrect to characterize the bedform field, at any given time, by ripples with a single characteristic spacing. Yet existing sediment transport models often tend to make these assumptions (i.e. Grant and Madsen, 1986; Fredsoe and Deigaard, 1992; Nielsen, 1992). As Grant and Madsen (1986, p. 288) state, the bed roughness is not known for multiple sets of ripples at oblique angles to the flow. The time scales of the observed changes also raise questions about model assumptions. We need to know more about the lag times between the development of a particular seabed state and changes in the hydrodynamic forcing, and if these lag times depend upon the previous state of the bed. Finally, it is interesting that the comparison between our observations of bedform transformations with time and Clifton's cross-shore progression yields both differences and similarities. This indicates that more general relationships between nearshore bedform properties and hydrodynamic forcing parameters, such as the grain roughness Shields parameter, will need to incorporate effects beyond those of the incident waves alone. In particular, the longshore current is bound to be important.

Acknowledgements

We thank Tony Bowen for providing the hydrodynamic data, Brian Greenwood for helpful discussions of his observations of bedforms in the nearshore, and Ed Clifton for useful criticism of the original manuscript. For their help at Burley Beach, we are grateful to A. Crawford, R. Dittman, B. Guest, and B. Roberts (Memorial University); D. Hazen, N. Countway, S. McLean, and A. Trivett (Dalhousie University); and R. Brander, T. Aagaard, R. Atkins, and K. Jagger (University of Toronto). One of us (DJW) was supported by a graduate fellowship from Memorial University of Newfoundland. This work was funded by the Operating and Strategic Grants programmes of the Natural Sciences and Engineering Research Council of Canada, and by the Office of Naval Research.

References

Allen, J.R.L., 1982a. Sedimentary Structures: Their Character and Physical Basis. Elsevier, Amsterdam, 1, 593 pp.

Allen, J.R.L., 1982b. Sedimentary Structures: Their Character and Physical Basis. Elsevier, Amsterdam, 2, 663 pp.

Clifton, H.E., 1976. Wave-formed sedimentary structures—A conceptual model. In: R.A. Davis, Jr. and R.L. Ethington (Editors), Beach and Nearshore Sedimentation. SEPM Spec. Publ., 24: 126–148.

Clifton, H.E. and Dingler, J.R., 1984. Wave-formed structures and paleoenvironmental reconstruction. Mar. Geol., 60: 165–198.

Clifton, H.E., Hunter, R.E. and Phillips, R.L., 1971. Depositional structures and processes in the non-barred high-energy nearshore, J. Sediment. Petrol., 41: 651–670.

Dingler, J.R. and Inman, D.L., 1976. Wave-formed ripples in nearshore sands. Proc. 15th Conf. Coastal Eng., pp. 2109–2126.

Dingler, J.R. and Clifton, H.E., 1984. Tidal cycle changes in oscillation ripples on the inner part of an estuarine sand flat. Mar. Geol., 60: 219–233.

Fredsoe, J. and Deigaard, R., 1992. Mechanics of Coastal Sediment Transport. World Scientific, River Edge, NJ, 369 pp.

Grant, W.D. and Madsen, O.S., 1986. The continental shelf bottom boundary layer. Ann. Rev. Fluid Mech., 18: 265–305.

Greenwood, B., Richards, R.G. and Brander, R., 1993. Acoustic imaging of seabed geometry: A High Resolution Remote Tracking Sonar (HRRTS II). Mar. Geol., 112: 207–218.

Guza, R.T. and Thornton, E.B., 1980. Local and shoaled comparisons of sea surface elevations, pressures, and velocities. J. Geophys. Res., 85: 1524–1530.

Hay, A.E. and Bowen, A.J., 1993. Spatially correlated depth changes in the nearshore zone during autumn storms. J. Geophys. Res., 98(C7): 12,387–12,404.

Hay, A.E. and Bowen, A.J., 1994. On the spatial coherence scales of wave-induced suspended sand concentration fluctuations. J. Geophys. Res., in press.

Hay, A.E. and Sheng, J., 1992. Vertical profiles of suspended sand concentration and size from multifrequency acoustic backscatter. J. Geophys. Res., 97: 15,661–15,677.

Hay, A.E., Huang, L., Colbourne, E.B., Sheng, J. and Bowen, A.J., 1988. A high speed multi-channel data acquisition system for remote acoustic sediment transport studies. Proc. Oceans '88, Baltimore, pp. 413–418.

Horikawa, K. (Editor), 1988. Nearshore Dynamics and Coastal Processes, Theory, Measurement, and Predictive Models. Univ. Tokyo Press, Tokyo.

Hunter, R.E., Clifton, H.E. and Philips, R.L., 1979. Depositional processes, sedimentary structures, and predicted vertical sequences in barred nearshore systems, Southern Oregon Coast, J. Sediment. Petrol., 49: 711–726.

Miller, M.C. and Komar, P.D., 1980. A field investigation of the relationship between oscillation ripple spacing and the near-bottom water orbital motions. J. Sediment. Petrol., 50: 183–191.

Nielsen, P., 1981. Dynamics and geometry of wave-generated ripples. J. Geophys. Res., 86: 6467–6472.

Nielsen, P., 1992. Coastal Bottom Boundary Layers and Sediment Transport. World Scientific, River Edge, NJ, 324 pp.

Southard, J.B., Lambie, J.M., Pile, H.T. and Weidman, C.R., 1990. Experiments on bed configuration in fine sands under bidirectional purely oscillatory flow, and the possible origin of hummocky cross-stratification. J. Sediment. Petrol., 60: 1–17.